Electronic Supplementary Information (ESI)

Direct and Converse Piezoelectric Responses at the Nanoscale from Epitaxial $BiFeO_3$ Thin Films Grown by Polymer Assisted Deposition

José Manuel Vila-Fungueiriño*[a], Andrés Gómez*[b], J. Antoja-Lleonart[e], Jaume Gázquez[b], César Magén[c,d], B. Noheda[e] and Adrián Carretero-Genevrier*[a]

[a.] *Institut d'Électronique et des Systèmes (IES), UMR 5214, CNRS – Université de Montpellier, 860 rue Saint Priest, 34095 Montpellier, France. e-mail: adrien.carretero@ies.univ-montp2.fr, jose-manuel.vila@ies.univ-montp2.fr*

[b.] *Institut de Ciència de Materials de Barcelona ICMAB, Consejo Superior de Investigaciones Científicas CSIC, Campus UAB 08193 Bellaterra, Catalonia, Spain. e-mail: agomez@icmab.es*

[c.] *Instituto de Ciencia de Materiales de Aragón (ICMA), Universidad de Zaragoza-CSIC, Facultad de Ciencias, Universidad de Zaragoza, Pedro Cerbuna 12, 50009 Zaragoza, Spain.*

[d.] *Laboratorio de Microscopías Avanzadas (LMA), Instituto de Nanociencia de Aragón (INA), Universidad de Zaragoza, Mariano Esquillor, Edificio I+D, 50018 Zaragoza, Spain.*

[e.] *Zernike Institute for Advanced Materials, University of Groningen, Nijenborgh 4, 9747 AG Groningen, The Netherlands.*

Formation of hematite at high temperature synthesis

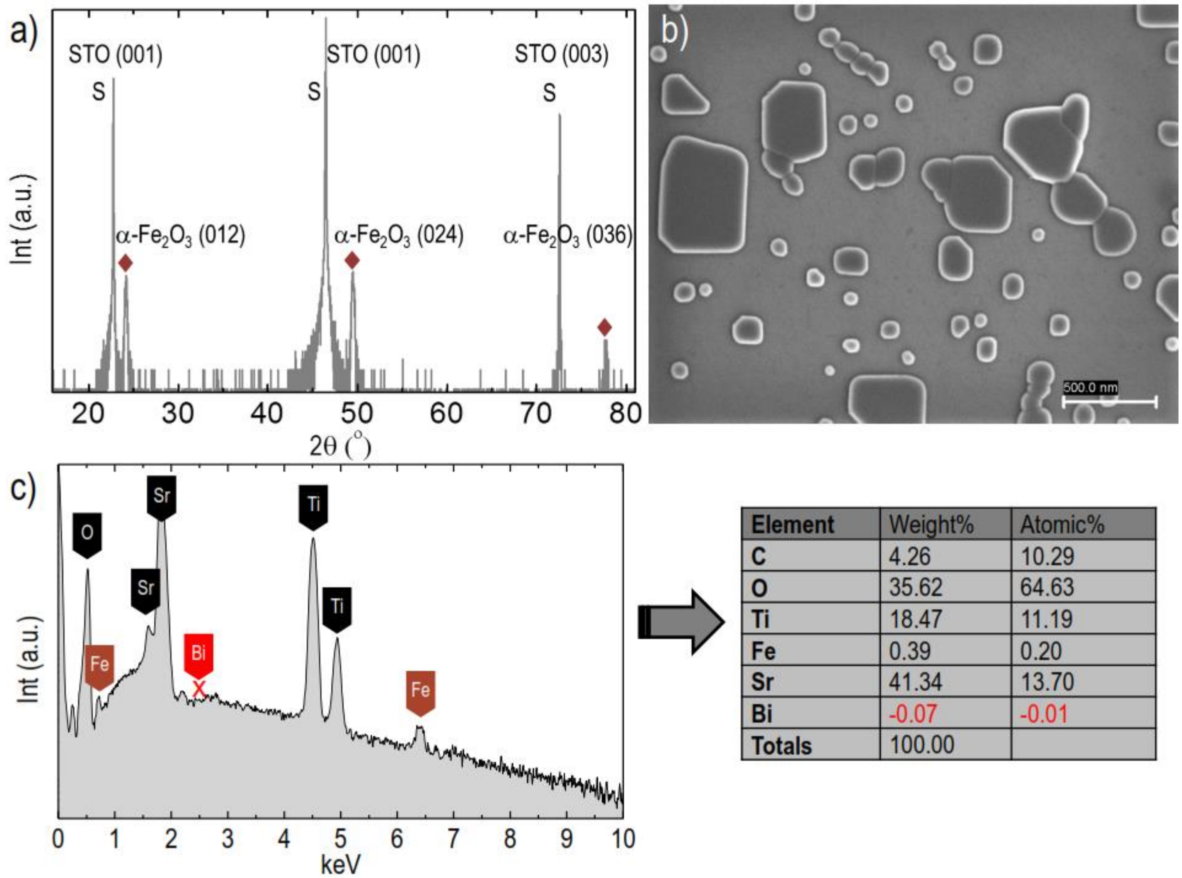

Element	Weight%	Atomic%
C	4.26	10.29
O	35.62	64.63
Ti	18.47	11.19
Fe	0.39	0.20
Sr	41.34	13.70
Bi	-0.07	-0.01
Totals	100.00	

Figure S1. a) XRD pattern of a sample annealed at 900°C showing the peaks corresponding to the STO substrate and the hematite phase. b) SEM image of this sample, where the iron oxide outgrowths can be observed. c) EDX analysis and elemental quantification of the elements present in the film.

X-Rays diffraction and reflection study of the temperature annealing dependence of BFO films

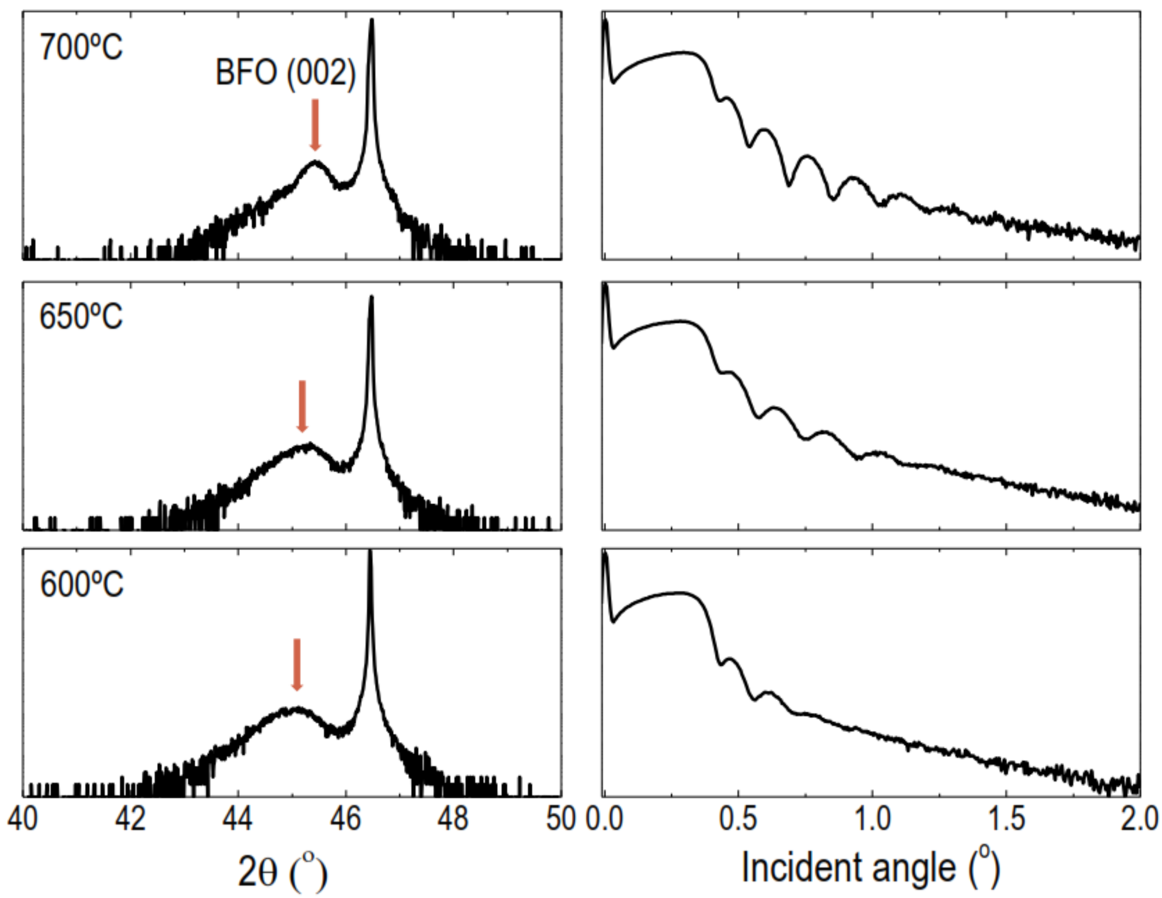

Figure S2. a) XRD patterns around the (002) peak (left) and XRR curves (right) of 23 nm-thick BFO thin films annealed at 600, 650, and 700°C showing the peaks corresponding to the STO substrate and the BFO phase. The corresponding out-of-plane lattice parameters for BFO films are $c_{BFO}^{600} = 4.011$ Å, $c_{BFO}^{650} = 4.012$ Å, and $c_{BFO}^{700} = 3.999$ Å.

Epitaxial relationship between BFO thin film and STO substrate

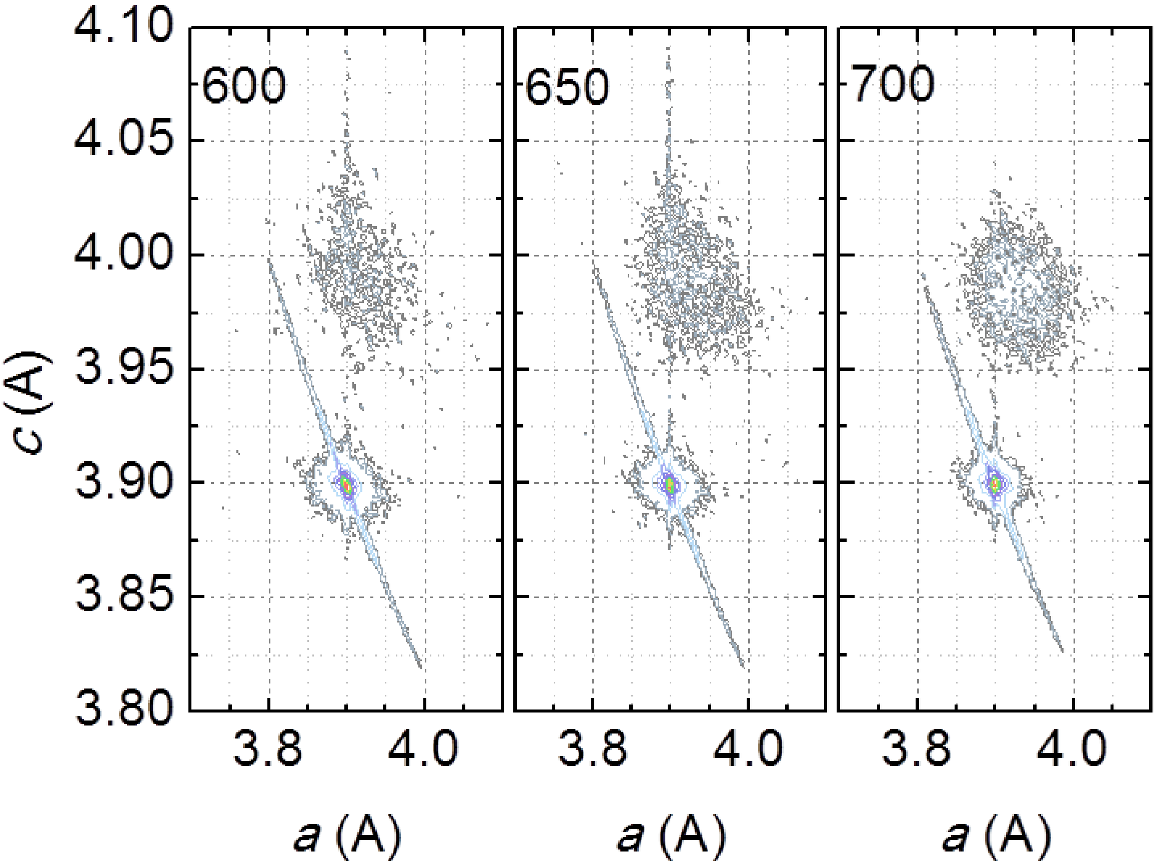

Figure S3. RSM of BFO thin films growth at different temperatures in which can be observed the compressive strain imposed by the substrate on the BFO.

Surface characterization of BFO films growth at different temperatures

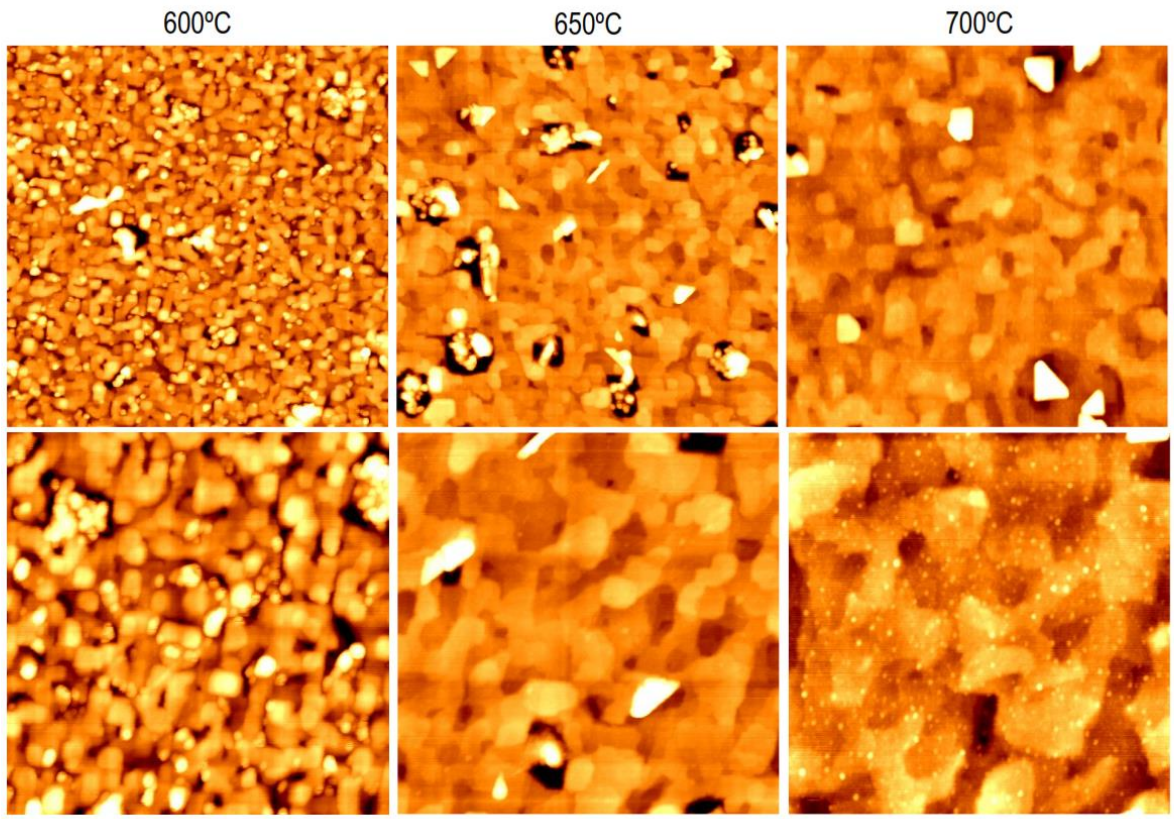

Figure S4. Atomic Force Microscopy imaging (5 × 5 µm; up) and (1 × 1 µm; bottom) of BFO films grown at 600, 650, and 700°C. The corresponding roughness values (R_q) for BFO films are 2.71 nm, 2,55 nm and 1.16 nm, respectively.

Synchrotron diffraction study of the crystallinity

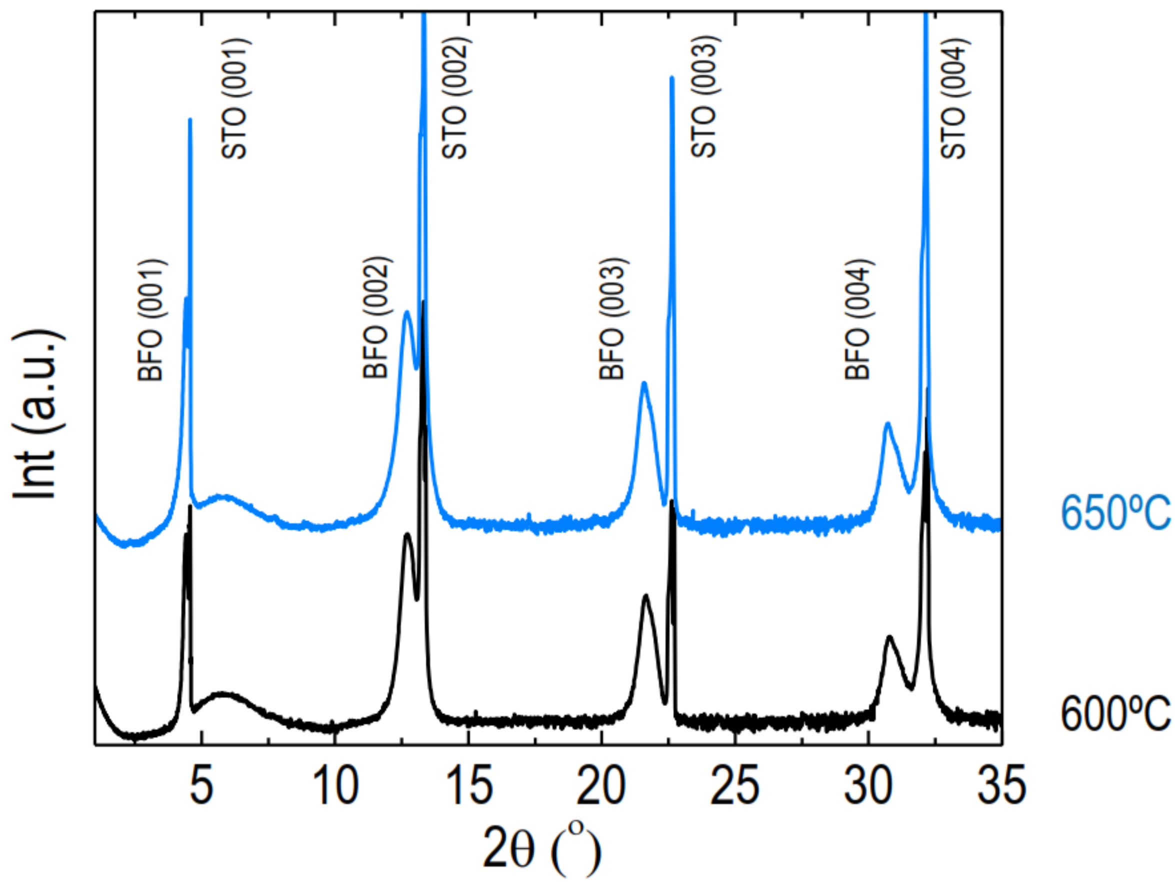

Figure S5. Synchrotron XRD pattern for 600°C and 650°C annealed BFO thin film in a θ-2θ configuration.

High Angle Annular Dark Field (HAADF) imaging in high-resolution STEM mode

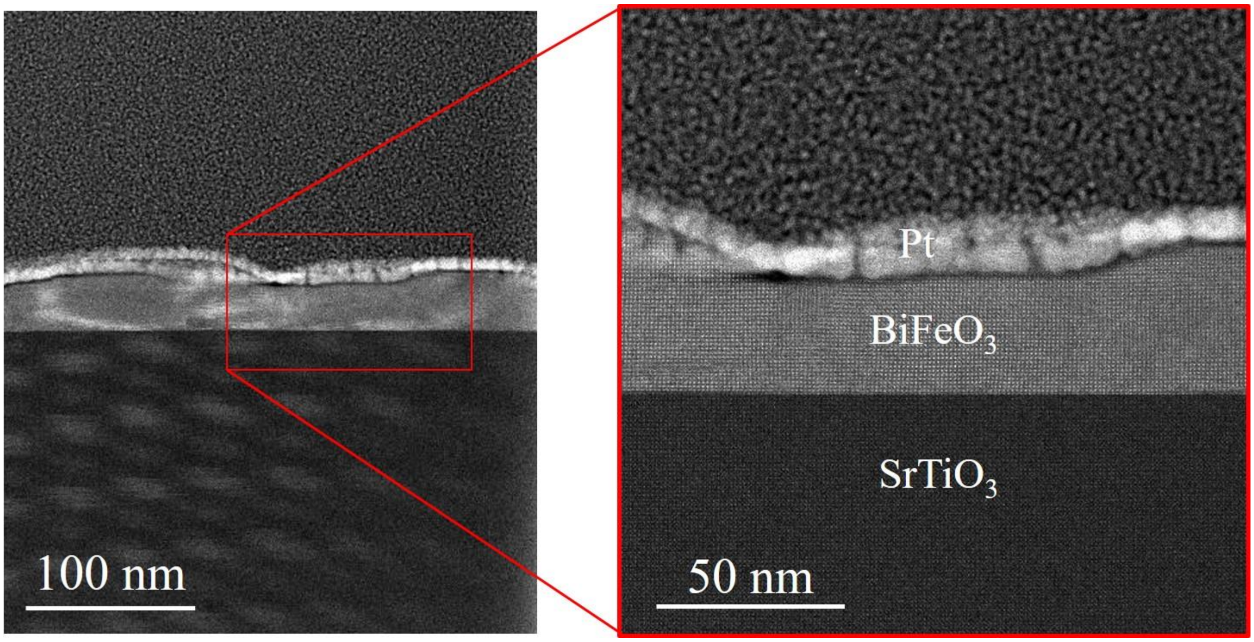

Figure S6. Low resolution and large Atomic resolution HAADF-STEM images of the 30 nm thick epitaxial BFO film viewed along the [100]-crystallographic direction.

Specific domain distribution of BFO films

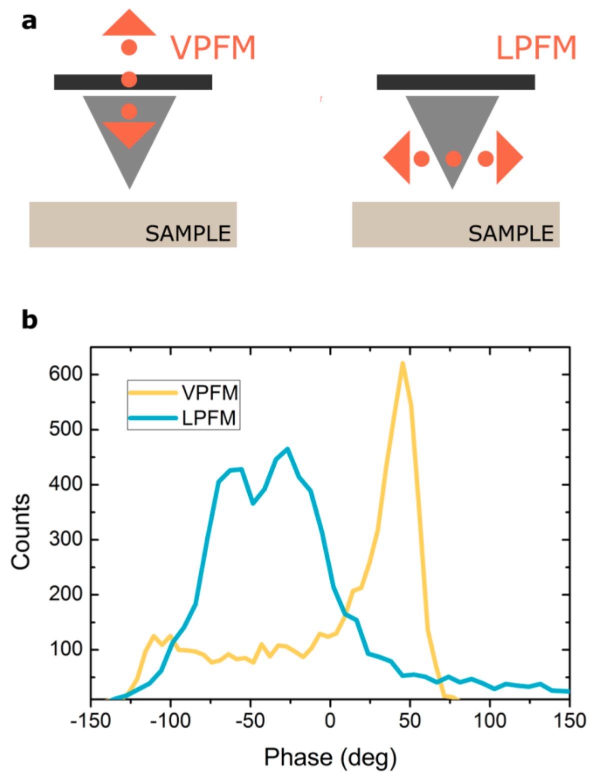

Figure S7. a. Schematic representation of Vertical PFM and Lateral PFM signals. The VPFM component provides information into the out-of-plane component of the polarization while the in-plane component is mapped through LPFM. b**.** Lateral and Vertical PFM phase histograms obtained from their corresponding PFM phase images, Figures 3b and 3d. From this data, it is obtained the most favorable domain structure from an energetic point of view. The 0-180º polarizations of BFO provide no signal into the in-plane channel, while the 71º orientation provides no signal into the out-of-plane polarization. The histograms show a clear signal in both channels, meaning that the most energetically favorable 109º domain configuration is predominant.

Growth of LSMO bottom electrode and BFO/LSMO heterostructure

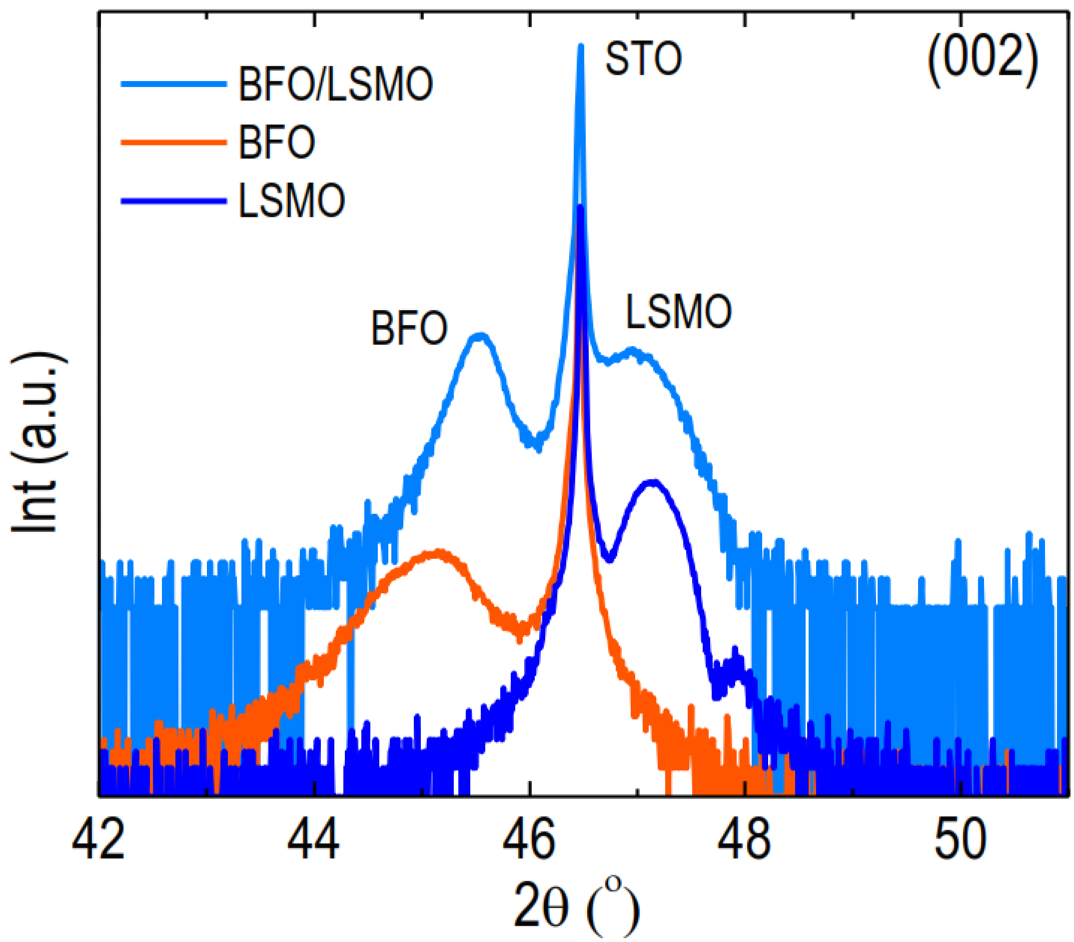

Figure S8. a) XRD patterns around the (002) peak of BFO thin film, LSMO thin film and BFO/LSMO multilayer.

High Angle Annular Dark Field (HAADF) imaging in high-resolution STEM mode of BFO/LSMO/STO heterostructure.

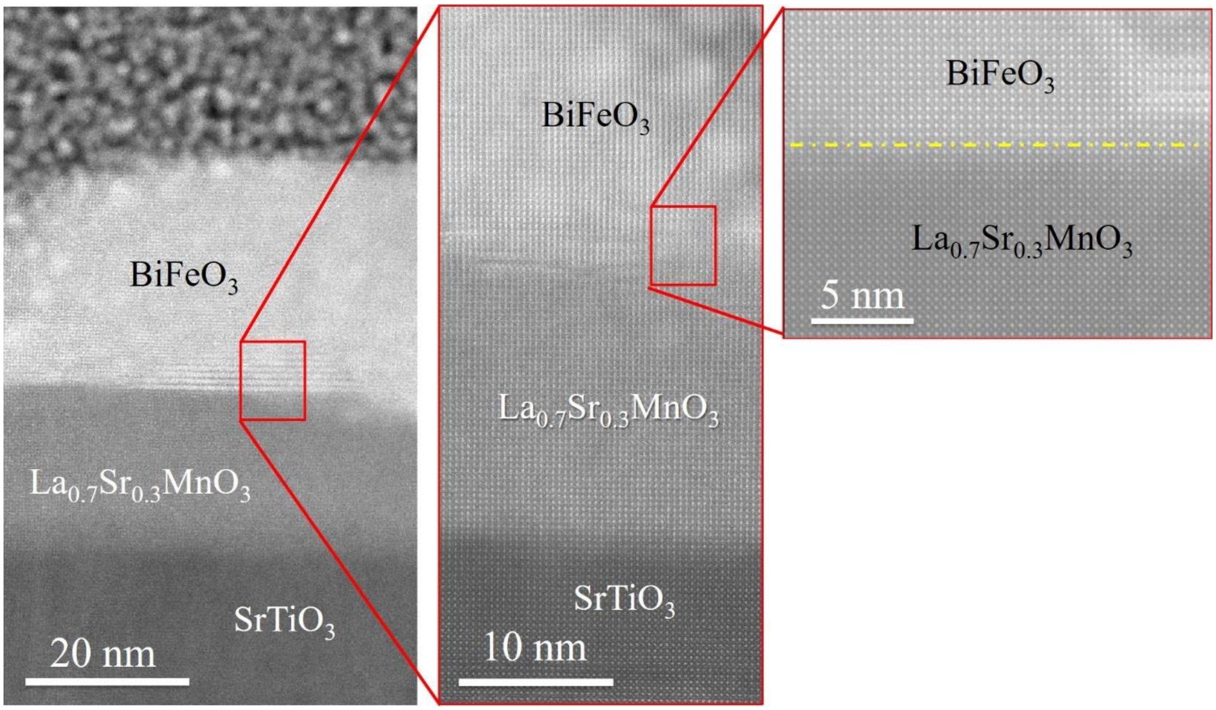

Figure S9. a) Atomic resolution HAADF-STEM image of the BFO/LSMO/STO oxide heterostructure viewed along the [100]-crystallographic direction. Detail of the HAADF image showing the coherent interface between the BFO and the LSMO bottom electrode (right image).

Ferroelectric poling of the 30 nm thick BFO sample

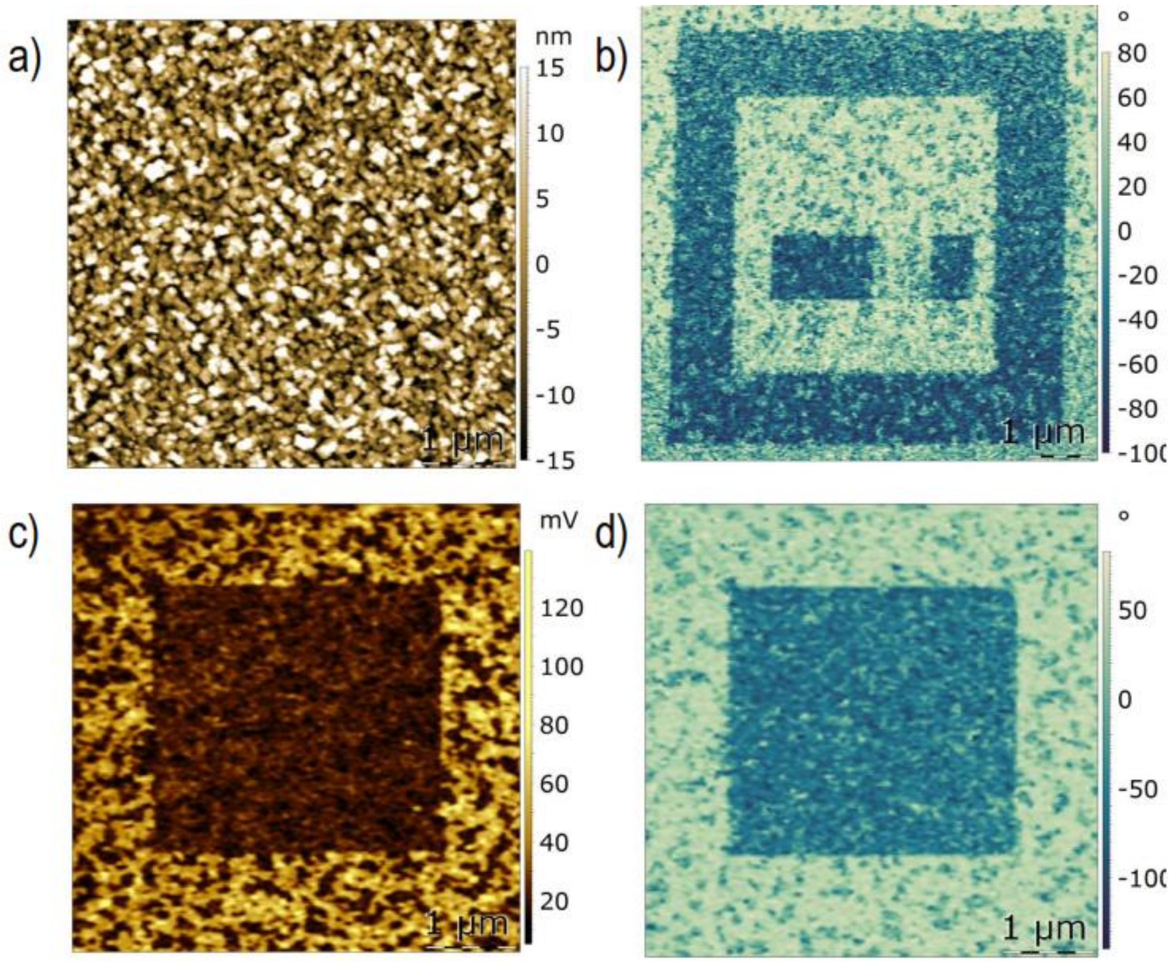

Figure S10. Ferroelectric poling acquired with PFM technique in 30 nm thick epitaxial BFO films grown over a bottom conductive LSMO electrode. a) Topography, b) PFM Phase, c) PFM Amplitude and d) PFM Phase, respectively, of pre-poled area, in which different squared patterns were recorded.

Phase and Amplitude vs DC bias applied, for a fixed AC magnitude

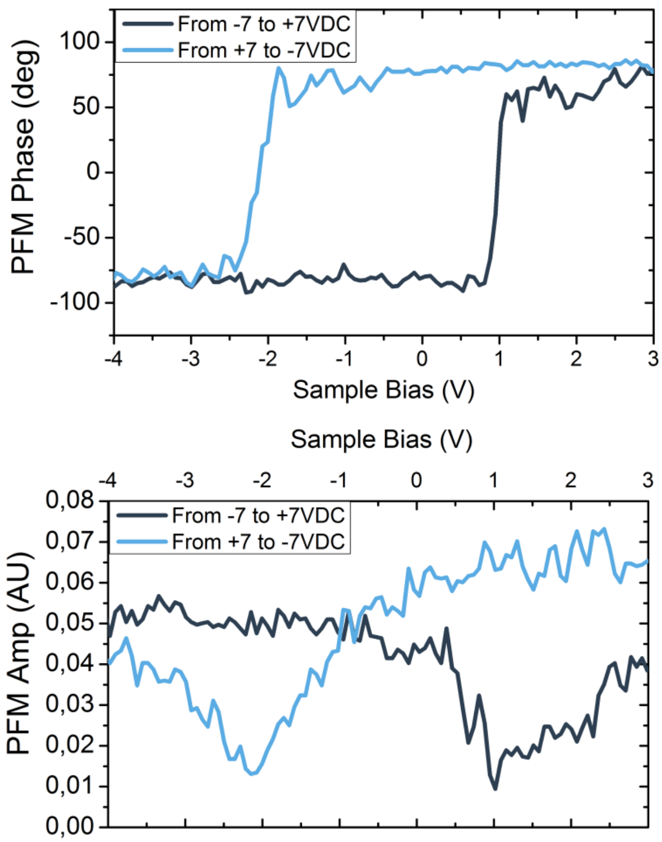

Figure S11. Phase and Amplitude vs DC bias applied for a fixed AC magnitude.

Switching spectroscopies obtained for the 60 nm thick epitaxial BFO films

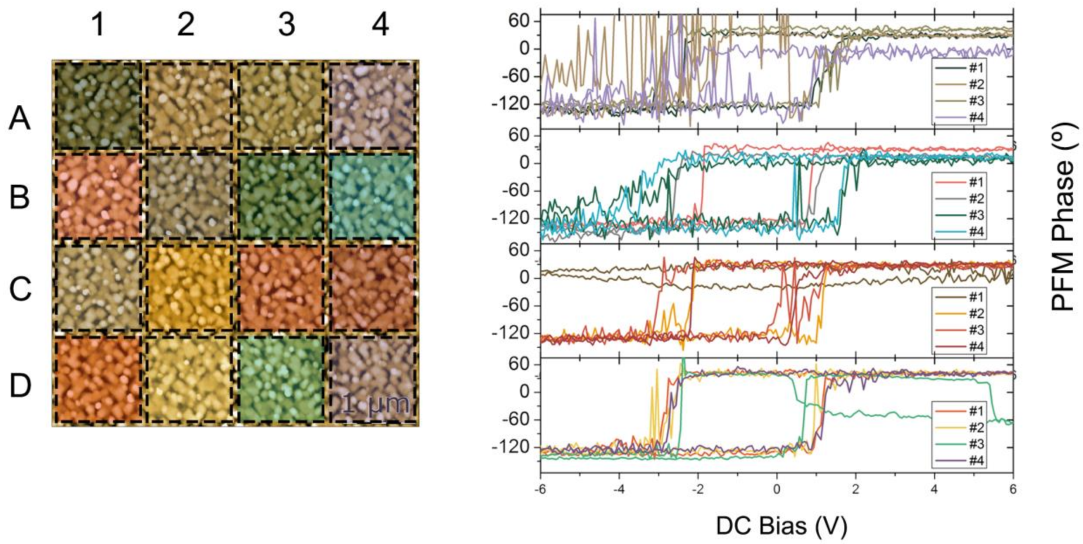

Figure S12. Switching spectroscopies obtained for the 60 nm thick epitaxial BFO films grown over a bottom conductive $La_{0.7}Sr_{0.3}MnO_3$ (LSMO) electrode. In this test, a matrix array of 4×4 spectroscopy curves are performed in a 5 × 5 µm area, in which the DC bias was swept from 0 VDC to +7 VDC then to −7 VDC and finishing at +7 VDC. The full cycle is depicted in all the measurements carried out, despite the highly localized measurements conditions. Note that all the curves in this file were included without any data manipulation, selection, filtering or extraction, proving the high homogeneity of our films.

Macroscopic measurements of (J–E) characteristics of 40 nm thick $BiFeO_3$ thin film

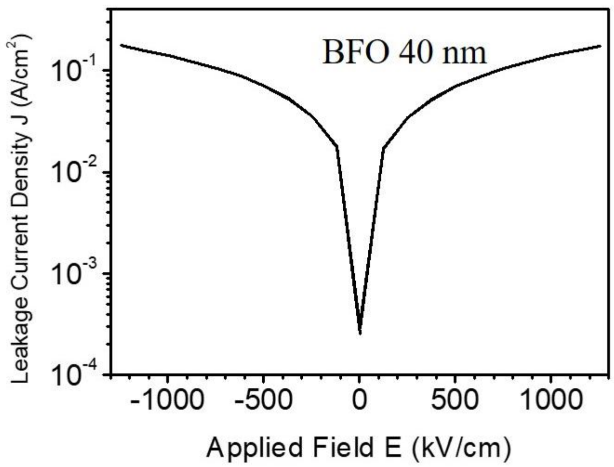

Figure S13. Macroscopic measurements of (J–E) characteristics of 40 nm thick $BiFeO_3$ thin film.